# ALMA Memo XXX
# Bandpass Calibration for ALMA

A.Bacmann (ESO) and S.Guilloteau (IRAM / ESO)

September 29, 2004

**Abstract**

This memo contains a detailed evaluation of the expected performance of the bandpass calibration for ALMA. We evaluate the limitations on the bandpass accuracy due to the imperfect knowledge of the atmospheric transmission. We show that the best bandpass accuracy is obtained when the amplitude calibration is applied in a single-load scheme. The proposed scheme is a variant of the so-called bandpass normalization technique. It uses normalization by the difference between the sky emission and the load emission, rather than normalization by the auto-correlation spectrum in the usual case. Bandpass calibration should be performed at the observing frequency. It will be limited by the knowledge of the sideband opacity difference. This knowledge can be based on a model, but a direct measurement is also possible, although time consuming.

The bandpass calibration must be performed on strong point-like sources, of known spectral index. The knowledge of the spectral indexes will be a limiting factor in the wide band modes. Building up a database of suitable sources will be necessary, since the knowledge of these spectral indexes could be improved by bootstrapping techniques among several sources. Since astronomical sources have to be used, the required integration time varies substantially as a function of frequency. High accuracies can be reached in a minute of time at mm wavelengths, but integration time as large as an hour can be needed at sub-mm wavelengths. Occasional direct measurements of the sideband opacity difference could also be used to improve the accuracy of the atmospheric modelling.

## 1 Basic Principles

The ALMA acquisition system is made of several elements which have frequency-dependent responses. From the sky to the detector (the correlator), the signal path encounters the following items:

- the atmosphere (especially close to absorption lines).
- the antennas.
- the receivers. Most ALMA receivers have a 4-12 GHz IF output. Millimeter receivers will be Single Side Band (SSB, with rejections of $\sim$15 dB) whereas submillimeter receivers will be Double Side Band (DSB, sideband gain ratio $\simeq 1$).
- the down-converters. They convert the 4-12 GHz signal coming from the receiver into 4 bands between 2 and 4 GHz. The signal is first separated by a filter into one 4-8 GHz signal and one 8-12 GHz signal. The signal is then mixed with the signal of a tunable Local Oscillator (LO2), down converted and then filtered between 2 and 4 GHz. There are 2 down-converters per antenna, one for each polarization.

- the digitizers.
- the digital filters. These depend on the configuration selected by the users. It is in principle possible to calculate the filters response to a given signal, but some peculiar effects like the Gibbs phenomenon depend on the signal itself.

The system is pictured in Fig. 1.

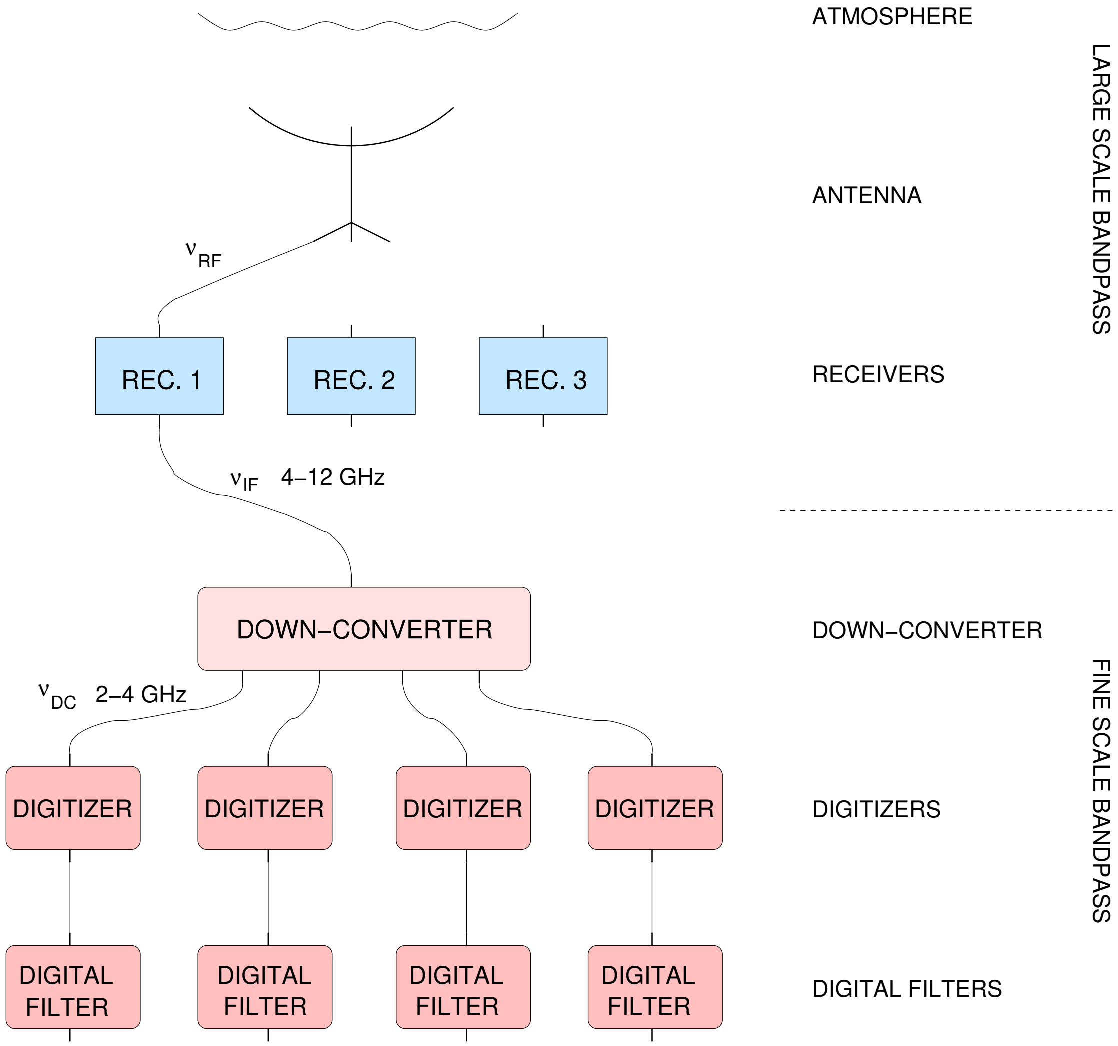


Figure 1: Acquisition system with frequency dependent elements.

The total (complex) **voltage** gain $U$ of one antenna can be written as the product of the gains from each single element, as function of frequency:

$$U(\nu_{RF}) = u_{\rm atm}(\nu_{RF})u_{\rm ant}(\nu_{RF})u_{\rm rec}(\nu_{RF})u_{\rm IF}(\nu_{IF})u_{\rm DC}(\nu_{DC})u_{\rm DF}(\nu_{DF}) \qquad (1)$$

where $\nu_{RF}$ is the sky frequency, $\nu_{IF}$ the corresponding intermediate frequency (in the range 4-12 GHz), and $\nu_{DC}$ is the down-converted frequency (in the 2-4 GHz range since ALMA uses

bandpass sampling), and $\nu_{DF}$ is the final baseband frequency (in the range 0-X GHz where X the width of the digital filter) respectively (cf. Fig. 1). The various frequency-dependent gains are:
- $u_{\rm atm}$ the atmospheric transmission (time dependent)
- $u_{\rm ant}$ the antenna gain (time dependent), which includes the flux to antenna temperature conversion, and standing wave effects
- $u_{\rm rec}$ the receiver gain
- $u_{\rm IF}$ the IF chain gain (within the receiver)
- $u_{\rm DC}$ the down-converter gain
- $u_{\rm DF}$ the digital filter gain

For each voltage gain $u_{\rm item}$ (including $U$), there is a corresponding **power** gain $g_{\rm item}$ given by

$$g_{\rm item} = |u_{\rm item}|^2 \tag{2}$$

so that the power response at time $t$ is

$$G(\nu_{RF},t) = g_{\rm atm}(\nu_{RF},t)g_{\rm ant}(\nu_{RF},t)g_{\rm rec}(\nu_{RF},t)g_{\rm IF}(\nu_{IF},t)g_{\rm DC}(\nu_{DC},t)g_{\rm DF}(\nu_{DF},t) \tag{3}$$

The atmospheric transmission is out of our control, but the system can be designed so that the receiver, IF chain and down-converter frequency responses become (to first order) time independent. Also, the antenna chromatism is mostly linked to standing wave effects and can be made small. We shall ignore it in the following discussions. In the calibration process, we shall assume that there is no closure error, so that the overall calibration can be made on an antenna basis. Phase closure is easy to obtain with a digital correlator, but amplitude closure is only obtained provided decorrelation effects and bandpass mismatches are small. Closure will thus be obtained provided the individual integration times are not excessive, and the total bandwidth is analyzed in sufficiently narrow chunks. Finally, the digital filter response can be computed and corrected for in real time. So, in summary we make the following **Assumptions**

1. Calibration is Antenna based. Closure errors are negligible.
2. The intrinsic frequency response of the system is stable: $g_{\rm rec}(\nu_{RF},t) = g_{\rm rec}(\nu_{RF})\gamma_{\rm rec}(t)$ (ibid for $g_{\rm IF}$ and $g_{\rm DC}$)
3. Digital filters are pre-calibrated: $g_{\rm DF}(\nu_{DF},t) = 1$
4. Antenna chromatism is negligible: $g_{ant}(\nu_{RF},t) = \gamma_{\rm ant}(t)$

In this case, Eq.3 becomes

$$G(\nu_{RF},t) = g_{\rm atm}(\nu_{RF},t)\gamma_{\rm ant}(t)g_{\rm rec}(\nu_{RF})\gamma_{\rm rec}(t)g_{\rm IF}(\nu_{IF})\gamma_{\rm IF}(t)g_{\rm DC}(\nu_{DC})\gamma_{\rm DC}(t) \tag{4}$$

$$G(\nu_{RF},t) = g_{\rm atm}(\nu_{RF},t)g_{\rm rec}(\nu_{RF})g_{\rm IF}(\nu_{IF})g_{\rm DC}(\nu_{DC})\gamma_{\rm all}(t) \tag{5}$$

The calibration process works out by decomposing the time dependent, chromatic gain in a product of an achromatic, time dependent gain and of a time **independent**, chromatic gain called the **Bandpass**. Since the atmosphere includes a time dependent chromaticity (see Eq.5), it is clear that this arbitrary decomposition will only work provided we can adequately predict and correct for this component.

The baseline-based visibility gain is given as

$$G_{ij}(t,\nu) = U_i(t,\nu)U_j^*(t,\nu) \tag{6}$$

Each antenna gain can be decomposed in a frequency independent gain, $\mathcal{A}_i(t)$ and of a (eventually time dependent) bandpass function $\mathcal{B}_i(\nu,t)$, so that

$$G_{ij}(t,\nu) = \mathcal{A}_i(t)\mathcal{A}_J^*(t)\mathcal{B}_i(\nu,t)\mathcal{B}_j^*(\nu,t) \tag{7}$$

### 1.1 Amplitude Bandpass

For the autocorrelation, the **power** gain of an antenna is thus given by

$$G_i(t,\nu) = |\mathcal{A}_i(t)|^2|\mathcal{B}_i(\nu,t)|^2 = A_i(t)B_i(\nu,t) \tag{8}$$

so that the modulus of the visibility gain is

$$G_{ij}(t,\nu) = \sqrt{G_i(t,\nu)G_j(t,\nu)} \tag{9}$$

Comparison of equations 5 and 8 shows that the (antenna) amplitude bandpass term $B(\nu_{RF},t)$ is given by

$$B(\nu_{RF},t) = \frac{g_{\mathrm{atm}}(\nu_{RF},t)\gamma_{\mathrm{all}}(t)}{A(t)} g_{\mathrm{rec}}(\nu_{RF})g_{\mathrm{IF}}(\nu_{IF})g_{\mathrm{DC}}(\nu_{DC}) \tag{10}$$

If accurate enough predictions of the frequency dependence of the atmospheric transmission can be made **and applied in real time**, then $(g_{\mathrm{atm}}(\nu,t) = g_{\mathrm{atm}}(t))$, and we have

$$g_{\mathrm{atm}}(\nu_{RF},t)\gamma_{\mathrm{all}}(t) = A(t)$$

so that the bandpass term is constant in time and equal to

$$B(\nu_{RF}) = g_{\mathrm{rec}}(\nu_{RF})g_{\mathrm{IF}}(\nu_{IF})g_{\mathrm{DC}}(\nu_{DC}) \tag{11}$$

### 1.2 Phase Bandpass

The phase terms appearing in $\mathcal{B}_i(\nu,t)$ must also be calibrated out. The first order effect in the phase bandpass is the delay, which is the derivative of the phase versus frequency. In addition, filters introduce frequency dependent phases which must be calibrated out (see ALMA memo 452 by d'Addario). In order to obtain a time independent phase bandpass, it is important to properly correct for the time varying effects. A systematic effect is the geometrical delay, whose correction requires accurate baseline measurements. Delay errors due to digital truncation of the delay steps are entirely predictable and must be corrected for in software. The remaining dominant effect is the so-called "atmospheric phase", which is actually a delay, except near strong atmospheric lines, where there is an additional chromatic effect on the phase. The "phase" calibration of ALMA should actually correct for all atmospheric **delay** fluctuations. However, since the prediction of the variations of the atmospheric delay will inevitably be limited, the remaining uncorrected component will unavoidably introduce a variable bandpass. On long integrations, it will average to zero, but on short timescales (e.g. snapshot images) it may have a non-zero component.

## 2 Amplitude Bandpass Calibration

In the previous section, we introduced the bandpass in its simplest conceptual form, i.e. expressing the measured amplitude of visibility as the product of the source visibility by the baseline gain. However, this is not always the most appropriate representation because 1) the gain may have very fine frequency dependence, and 2) the atmosphere chromatism needs to be predicted and corrected for accurately. Because of the latter problem, the bandpass calibration depends on how the (time dependent) amplitude calibration (called Amplitude Calibration thereafter) is implemented. Actually, if the Amplitude Calibration could be done with the adequate spectral resolution, there would be no need for a subsequent bandpass calibration. Unfortunately this approach can not be implemented because there is insufficient sensitivity at the highest spectral resolution to directly determine the gain.

Hence, Amplitude Calibration and Bandpass Calibration intimately interact. We shall restate here the properties of the two usual Amplitude Calibration methods which are foreseen to be implemented for ALMA namely the Single Load and Dual Load methods.

## 2.1 Basic Equations of Amplitude Calibration

The calibration can be derived from the output powers measured by the receiver on the sky $P_{\text{sky}}$ and when looking at a load $P_{\text{load}}$, compared to the correlated signal measured by the correlator, $C_{\text{source}}$:

$$\begin{aligned} P_{\text{sky}} &= K(T)(T_{\text{rec}} + J_{\text{sky}}) \\ P_{\text{load}} &= K(T)(T_{\text{rec}} + f J_{\text{load}} + (1-f) J_{\text{sky}}) \\ C_{\text{source}} &= K(T) g_s \eta e^{-\tau} T_A \end{aligned} \tag{12}$$

The coefficient $K(T)$ incorporates possible non linearity of the detector (receiver + amplifiers + backend). $f$ is the fraction of the beam filled by the load, and $\eta$ the forward efficiency (we neglect the dependency of the forward efficiency between the two sidebands, since this is expected to be about 0.2 % in the worst case). $g_s$ and $g_i$ are the normalized signal and image gain of the receivers $g_s + g_i = 1$. Note that, in terms of image to signal sideband gain ratio, $g$,

$$g_s = 1/(1+g) \quad \text{and} \quad g_i = g/(1+g) \tag{13}$$

The sky emissivity $J_{\text{sky}}$ is given by

$$\begin{aligned} J_{\text{sky}} = \; & g_s(\eta J^s_{\text{m}}(1-e^{-\tau_s}) + \eta J^s_{\text{bg}} e^{-\tau_s} + (1-\eta) J^s_{\text{spill}}) \\ & + g_i(\eta J^i_{\text{m}}(1-e^{-\tau_i}) + \eta J^i_{\text{bg}} e^{-\tau_i} + (1-\eta) J^i_{\text{spill}}) \end{aligned} \tag{14}$$

where $\tau_j$ is the sky opacity (at the current elevation) and

$$J^j_{\text{x}} = \frac{h\nu_j}{k} \frac{1}{e^{h\nu_j/kT_{\text{x}}} - 1} \tag{15}$$

is the Rayleigh-Jeans equivalent temperature of a black body at $T_{\text{x}}$ at frequency $\nu_j$. $j$ takes values $s$ or $i$ for signal or image bands respectively. $J_{\text{m}}$ is the effective sky temperature, $J_{\text{bg}}$ the cosmic background, and $J_{\text{spill}}$ the spillover. Similarly, the effective load temperature $J_{\text{load}}$ is

$$J_{\text{load}} = g_s J^s_{\text{load}} + g_i J^i_{\text{load}} \tag{16}$$

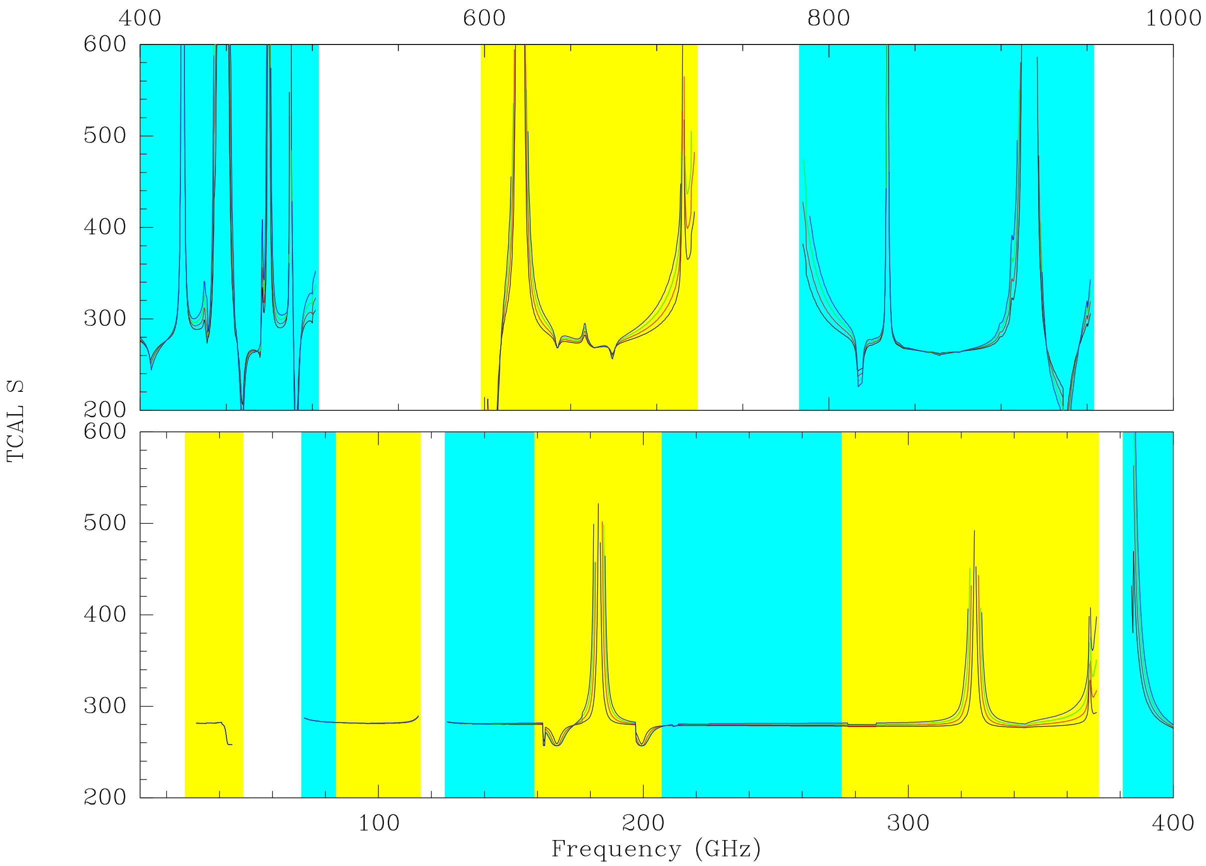


Figure 2: Dependency of the $T_{\rm cal}/(1+g)$ factor as function of frequency for a load temperature of 283 K in the single-load calibration scheme. Curves are given for 4 water vapor content: 0.5 mm (black), 1 mm (red), 1.5 mm (green) and 2 mm (blue) for frequencies below 380 GHz, and 0.35, 0.45, 0.55, 0.65 for frequencies above 380 GHz. The color shadings indicate the receiver bands. The colors are arbitrary.

### 2.2 Single Load Calibration

In the single-load technique, the source antenna temperature is given by

$$T_A = T_{\rm cal}\frac{C_{\rm source}}{P_{\rm load} - P_{\rm sky}} \tag{17}$$

where $T_{\rm cal}$ is the calibration temperature [Ulich & Haas, 1976]. From Eq.13, one can easily express $T_{\rm cal}$ as

$$\begin{aligned} T_{\rm cal} &= \frac{e^{\tau_s}}{\eta g_s} f(J_{\rm load} - J_{\rm sky}) && (18)\\ &= \frac{e^{\tau_s}}{\eta g_s} f(g_s J^s_{\rm load} + g_i J^i_{\rm load} \\ &- g_s(\eta J^s_{\rm m}(1-e^{-\tau_s}) + \eta J^s_{\rm bg} e^{-\tau_s} + (1-\eta) J^s_{\rm spill}) \\ &- g_i(\eta J^i_{\rm m}(1-e^{-\tau_i}) + \eta J^i_{\rm bg} e^{-\tau_i} + (1-\eta) J^i_{\rm spill})\ ) && (19) \end{aligned}$$

The coupling factor to the load, $f$, appears as a simple scaling factor in $T_{\rm cal}$, and will just be set to 1 in the following equations for simplicity. Eq.19, after some (tedious) re-arrangement is strictly equivalent to the following one

$$\begin{aligned}
T_{\rm cal} &= J^s_{\rm spill} - J^s_{\rm bg} + g(J^i_{\rm spill} - J^i_{\rm bg}) \\
&+ (e^{\tau_s} - 1)(J^s_{\rm spill} - J^s_{\rm m} + g(J^i_{\rm spill} - J^i_{\rm m})) \\
&+ g(e^{\tau_s - \tau_i} - 1)(J^i_{\rm m} - J^i_{\rm bg}) \\
&+ \frac{e^{\tau_s}}{\eta}(J^s_{\rm load} - J^s_{\rm spill} + g(J^i_{\rm load} - J^i_{\rm spill}))
\end{aligned} \tag{20}$$

Eq.20 allows to put in better perspective the effect of the various parameters. Eq.20 can further be (simply) re-arranged to explicitly separate two terms, one which depends on the opacity difference between the signal and image bands and one which does not.

$$\begin{aligned}
T_{\rm cal} &= J^s_{\rm spill} - J^s_{\rm bg} + g(J^i_{\rm spill} - J^i_{\rm bg}) \\
&+ (e^{\tau_s} - 1)(J^s_{\rm spill} - J^s_{\rm m} + g(J^i_{\rm spill} - J^i_{\rm m})) \\
&+ \frac{e^{\tau_s}}{\eta}(J^s_{\rm load} - J^s_{\rm spill} + g(J^i_{\rm load} - J^i_{\rm spill})) \\
&+ g(e^{\tau_s - \tau_i} - 1)(J^i_{\rm m} - J^i_{\rm bg})
\end{aligned} \tag{21}$$

Defining $X_{\rm source}$ as,

$$X_{\rm source}(\nu) = \frac{C_{\rm source}(\nu)}{P_{\rm load} - P_{\rm sky}(\nu)}. \tag{22}$$

we obtain

$$T_A(\nu) = T_{\rm cal}(\nu) X_{\rm source}(\nu) \tag{23}$$

### 2.3 Dual-Load Calibration

In the dual-load calibration system, a cold and a hot temperature loads are used in general.

$$P_{\rm hot} = K(T)(T_{\rm rec} + J_{\rm cold}) \tag{24}$$

$$P_{\rm hot} = K(T)(T_{\rm rec} + J_{\rm hot}) \tag{25}$$

$$C_{\rm source} = K(T) g_s \eta e^{-\tau} T_A \tag{26}$$

Eliminating the electronic gain $K(T)$ (ignoring saturation at this stage) gives

$$T_A = \frac{e^{\tau}}{g_s \eta}(J_{\rm hot} - J_{\rm cold}) \frac{C_{\rm source}}{P_{\rm hot} - P_{\rm cold}} = T_{\rm cal} \frac{C_{\rm source}}{P_{\rm hot} - P_{\rm cold}} \tag{27}$$

where the calibration temperature is now

$$T_{\rm cal} = \frac{(1+g)e^{\tau}}{\eta}(J_{\rm hot} - J_{\rm cold}) \tag{28}$$

Defining $X_{\rm source}$ as,

$$X_{\rm source}(\nu) = \frac{C_{\rm source}(\nu)}{P_{\rm hot} - P_{\rm cold}} \tag{29}$$

the antenna temperature $T_A$ is derived from $X$ by

$$T_A = T_{\rm cal}(\nu) X_{\rm source}(\nu) \tag{30}$$

The dependency of $T_{\rm cal}$ as a function of frequency for various water vapour contents is shown in Fig. 3 in the dual-load case.

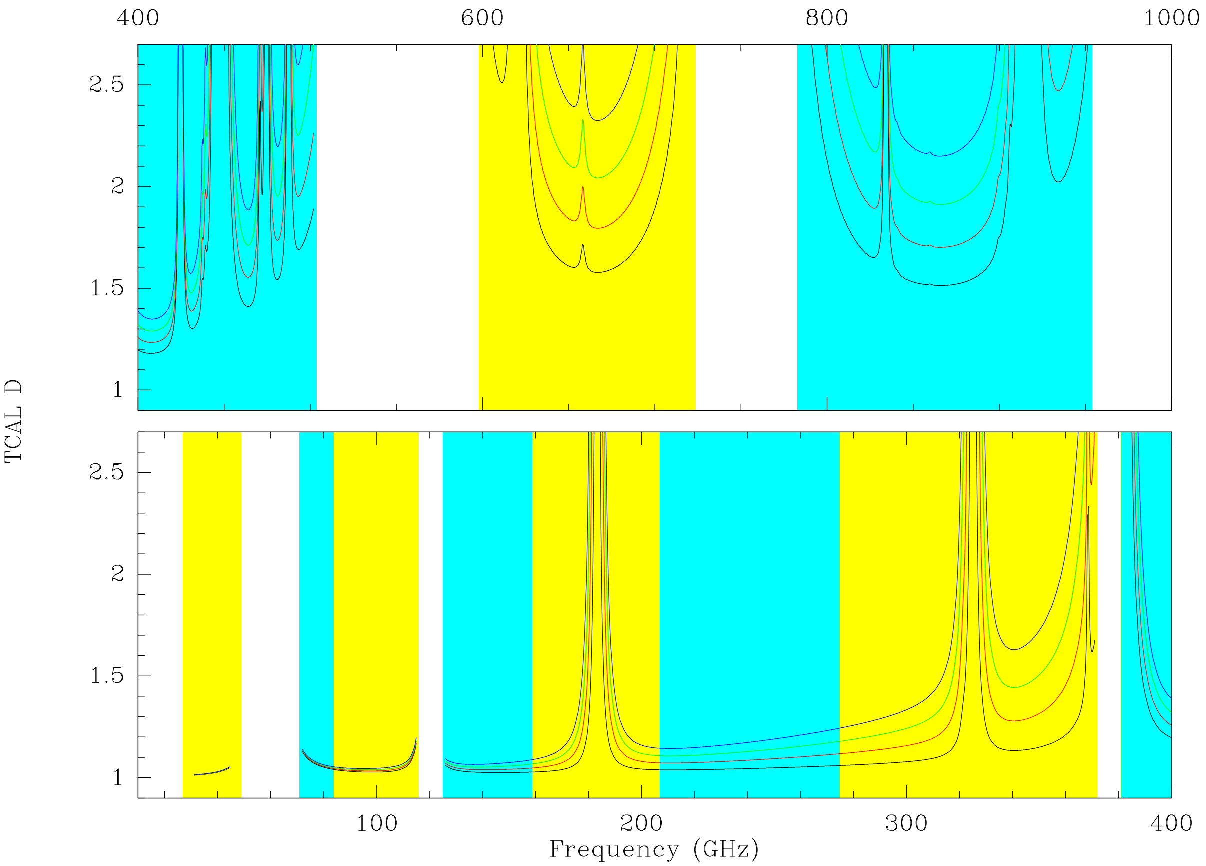


Figure 3: Dependency of the $T_{\rm cal}/(1+g)$ factor as function of frequency in the case of the dual-load calibration scheme. Curves are given for 4 water vapor content: 0.5 mm (black), 1 mm (red), 1.5 mm (green) and 2 mm (blue) for frequencies below 380 GHz, and 0.35, 0.45, 0.55, 0.65 for frequencies above 380 GHz. The value is given for $J_{\rm hot} - J_{\rm cold} = 1$ K.

### 2.3.1 Comparison and refinements

It can be seen from Fig. 2- 3 that the single load calibration method provides a more accurate way to calibrate the bandpass, since the $T_{\rm cal}$ factor is a rather smooth function of the frequency, and depends very little on the elevation or the water vapor content (Fig. 2). Most of the dependence in these parameters is carried out by the denominator $P_{\rm load} - P_{\rm sky}$ in Eq.17 and Eq.22.

Although it may look *a priori* surprising that a single-load can give better result than a dual-load, we should note that this is only true for the **bandpass** (or relative) calibration. **Absolute** calibration is better obtained with a dual-load system. In fact, if a dual-load system is available, it is possible to improve on the bandpass calibration by using a single-load scheme for the calibration, but adjusting the effective load temperature using a linear combination of the two loads such that

$$J_{\rm load} = (1-\eta) J_{\rm spill} + \eta J_{\rm m} \tag{31}$$

In this case, the calibration factor $T_{\rm cal}$ becomes

$$T_{\rm cal} = J_{\rm m} - J_{\rm bg} \tag{32}$$

However, it is likely that the adjustment of $J_{\rm load}$ can not be made continuously. In this case, our expressions of $T_{\rm cal}$ and its derivatives can still be used with the actual value of $J_{\rm load}$.

## 2.4 Bandpass Determination

### 2.4.1 Problem Definition

In both amplitude calibration methods, the antenna temperature is derived from a measured quantity $X$ by

$$T_{\rm source} = T_{\rm cal}(\nu) X_{\rm source}(\nu) \tag{33}$$

but the quantity $X$ and the expression of $T_{\rm cal}$ differ.

On a strong, unresolved, continuum source (called the "bandpass" calibrator), we thus have

$$T_{\rm bandpass} = T_{\rm cal}(\nu, w_b, a_b, x_b) X_{\rm bandpass}(\nu) = T_{\rm ref} \left(\frac{\nu}{\nu_{\rm ref}}\right)^{\alpha} \tag{34}$$

where $\alpha$ is the spectral index of the source (a power law spectrum is assumed here for simplicity). For simplification, we shall assume $\alpha = 0$ unless notified. In the above expression, $\nu$ is the observing frequency, $w_b$ the water vapor content during the measurement, $a_b$ the airmass of the observation, and $x_b$ other atmospheric parameter which is required to compute $T_{\rm cal}$ (subscript $b$ stand for "bandpass observation"). If we had computed $T_{\rm cal}$ from an accurate model and with the true values for the parameters, $T_{\rm bandpass}$ would indeed represent the true spectrum of the source.

However, we only computed $T_{\rm cal}$ at some given frequency, say $\nu_0$ (and/or with some limited spectral resolution), and with user specified values for the water vapor, $w_{b_0}$ (and perhaps other parameters $x_{b_0}$, but we are clever enough to use $a_{b_0} = a_b$). So what we have computed is actually:

$$T^0_{\rm bandpass}(\nu) = T_{\rm cal}(\nu_0, w_{b_0}, a_b, x_{b_0}) X_{\rm bandpass}(\nu) \tag{35}$$

and it has a frequency dependence. The bandpass $B(\nu)$ is the ratio between $T_{\rm ref}$ and $T^0(\nu)$, i.e.

$$B(\nu) = \frac{T_{\rm ref}}{T^0_{\rm bandpass}(\nu)} = \frac{T_{\rm cal}(\nu, w_b, a_b, x_b)}{T_{\rm cal}(\nu_0, w_{b_0}, a_b, x_{b_0})} \tag{36}$$

With similar notations, using subscript $s$ for the on source observation, the source antenna temperature is derived from

$$T^0_{\rm source}(\nu) = B(\nu) T_{\rm cal}(\nu_0, w_{s_0}, a_s, x_{s_0}) X_{\rm source}(\nu) \tag{37}$$

where $w_{s_0}$ is the assumed water vapor content, while the true value should be

$$T_{\rm source}(\nu) = T_{\rm cal}(\nu, w_s, a_s, x_s) X_{\rm source}(\nu) \tag{38}$$

Thus the bandpass error made during this measurement is

$$\begin{aligned} \frac{\delta B}{B} &= 1 - \frac{T_{\rm cal}(\nu, w_s, a_s, x_s) T_{\rm cal}(\nu_0, w_{b_0}, a_b, x_{b_0})}{T_{\rm cal}(\nu_0, w_{s_0}, a_s, x_{s_0}) T_{\rm cal}(\nu, w_b, a_b, x_b)} && (39) \\ &= 1 - Q(\text{source})/Q(\text{bandpass}) && (40) \end{aligned}$$

### 2.4.2 Development

Assuming the dependencies of $T_{\rm cal}$ as a function of $\nu$, $w$ and $a$ (and any other environmental parameter $x$) is small, we can expand $T_{\rm cal}$ as a function of its derivatives, and obtain the expression of $Q$

$$
\begin{aligned}
Q &= \frac{T_{\rm cal}(\nu, w, a, x)}{T_{\rm cal}(\nu_0, w_0, a, x_0)} && (41)\\
&= 1 + (\nu-\nu_0)\frac{1}{T_{\rm cal}}\frac{\partial T_{\rm cal}}{\partial \nu} + (w-w_0)\frac{1}{T_{\rm cal}}\frac{\partial T_{\rm cal}}{\partial w} + (x-x_0)\frac{1}{T_{\rm cal}}\frac{\partial T_{\rm cal}}{\partial x} && (42)\\
&= 1 + \Delta\nu Q_\nu + \delta w Q_w + \delta x Q_x && (43)
\end{aligned}
$$

where $Q_x$ is the logarithmic derivative of $T_{\rm cal}$ relative to $x$. We have noted $\Delta\nu$ the (known) difference between the $\nu$ and $\nu - \nu_0$, and $\delta x$ the (unknown) differences between $x$ and $x_0$. Only the variance of $\delta x$ is known. We are not interested in the absolute value of $B(\nu)$ (which is an amplitude calibration error and will be calibrated out as part of the $\gamma_{\rm all}(t)$ term), but only on its dependence on $\nu$. So the bandpass error can be expanded as

$$
\begin{aligned}
\frac{\delta B}{B} &= (\nu-\nu_0)((Q_\nu(a_s) - Q_\nu(a_b)) && (44)\\
&\quad +((w_s - w_{s_0})Q_w(a_s) - (w_b - w_{b_0})Q_w(a_b)) && (45)\\
&\quad +((x_s - x_{s_0})Q_x(a_s) - (x_b - x_{b_0})Q_x(a_b))) && (46)
\end{aligned}
$$

We have now to consider that, except for $\nu - \nu_0$, we are dealing with random variables, and interested in the average bandpass errors. For example, the error on the water vapor content $w_k - w_{k_0}$ is a random quantity. Also, since we are dealing with random effects here, we shall neglect for simplicity the dependence of the $Q_x$ on the airmass, and use a representative value for this. We can thus derive the bandpass error from

$$
\left(\frac{\delta B}{B}\right)^2 = (\nu-\nu_0)^2\left((Q_\nu(a_s) - Q_\nu(a_b))^2 + 2\delta w Q_w^2 + 2\delta x Q_x^2\right) \qquad (47)
$$

Let us consider the first term in more details and express it as a function of the partial derivative of $T_{\rm cal}$ with respect to $\nu$ and $a$.

$$
\begin{aligned}
Q_\nu(a_s) - Q_\nu(a_b) &\simeq (a_s - a_b)\frac{\partial Q_\nu}{\partial a} && (48)\\
&= (a_s - a_b)\frac{\partial}{\partial a}\left(\frac{1}{T_{\rm cal}}\frac{\partial T_{\rm cal}}{\partial \nu}\right) && (49)\\
&= (a_s - a_b)\left(\frac{1}{T_{\rm cal}}\frac{\partial^2 T_{\rm cal}}{\partial a \partial \nu} - \frac{1}{T_{\rm cal}^2}\frac{\partial T_{\rm cal}}{\partial a}\frac{\partial T_{\rm cal}}{\partial \nu}\right) && (50)\\
&= (a_s - a_b)\left(\frac{1}{T_{\rm cal}}\frac{\partial^2 T_{\rm cal}}{\partial a \partial \nu} - \frac{1}{T_{\rm cal}}\frac{\partial T_{\rm cal}}{\partial a}\times\frac{1}{T_{\rm cal}}\frac{\partial T_{\rm cal}}{\partial \nu}\right) && (51)
\end{aligned}
$$

Hence, the total bandpass error is

$$
\begin{aligned}
\left(\frac{\delta B}{B}\right)^2 &= (\Delta\nu)^2(\Delta a)^2\left(\frac{1}{T_{\rm cal}}\frac{\partial^2 T_{\rm cal}}{\partial a \partial \nu} - \frac{1}{T_{\rm cal}}\frac{\partial T_{\rm cal}}{\partial a}\times\frac{1}{T_{\rm cal}}\frac{\partial T_{\rm cal}}{\partial \nu}\right)^2 && (52)\\
&\quad +(\Delta\nu)^2\left(2(\delta w)^2\left(\frac{1}{T_{\rm cal}}\frac{\partial T_{\rm cal}}{\partial w}\right)^2 + 2(\delta x)^2\left(\frac{1}{T_{\rm cal}}\frac{\partial T_{\rm cal}}{\partial x}\right)^2\right) && (53)
\end{aligned}
$$

where $\Delta a$ is the difference in airmass between the source and the bandpass calibration.

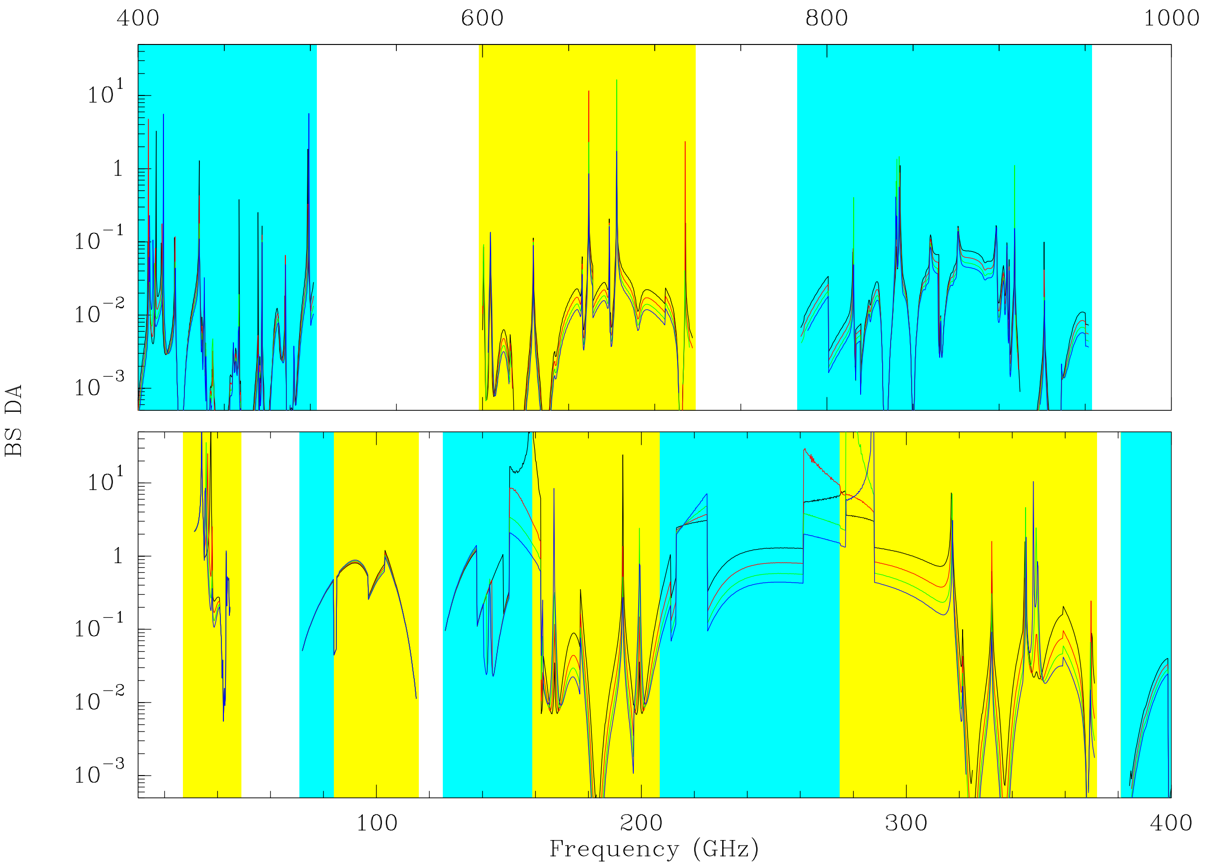


Figure 4: Maximum frequency offset to preserve a bandpass error of 0.1 % despite the elevation change between the source and the bandpass calibration for the Single Load calibration. The assumed elevation change is 0.5 airmass.

### 2.4.3 Interpretation

From Eq.53, it can be seen that the bandpass error depends linearly on the frequency offset between the observing frequency and the reference frequency used to compute $T_{\mathrm{cal}}$. Although in theory, $T_{\mathrm{cal}}$ can be computed with arbitrary frequency resolution, the measurements of $X_{\mathrm{source}}$ are made with finite resolution, in order to obtain adequate S/N. What is used in practice is a sampled value of $T_{\mathrm{cal}}$ in place of the appropriate bandwidth-averaged value which should be used instead. Eq.53 thus gives an estimate of (and more precisely a strict upper limit to) the bandpass error if $\Delta\nu$ is the step in frequency with which $T_{\mathrm{cal}}$ is computed.

Although an analytical derivation of the partial derivatives is possible, it is quite lengthy. Since we are interested in orders of magnitude of the errors, it is simpler to compute these as a function of frequency, for various typical observing conditions. We have computed these using the ATM model of Pardo and Cernicharo. Figures 4 to 8 present the resulting maximum allowable frequency offset ($F$ in GHz) to get a bandpass error of 0.1 % (0.001). All calculations were made assuming a single load temperature of 283 K, and an outside temperature of 273 K. The airmass of the source was assumed to be $\sqrt{2}$. The 4 curves represent 4 different values of the water vapor content: 0.5, 1, 1.5, 2 mm for frequencies below 380 GHz, and 0.35, 0.45, 0.55, 0.65 mm for frequencies above 380 GHz. The colored zones indicate the boundaries of the ALMA frequency bands.

Since the bandpass error is proportional to the frequency offset, these figures can simply be used to obtain the maximum bandpass error $b$ over a given bandwidth $\Delta\nu$: $b = 0.001\Delta\nu/F$. Scaling for different values of the other errors can be made in the same way. Figures 4-8 were derived using the best possible frequency setup with ALMA receivers: the selection of USB vs LSB (when possible) was made in order to minimize the image band opacity. This results in apparent discontinuities as function of frequency, when the selected band changes from USB to LSB and vice-versa.

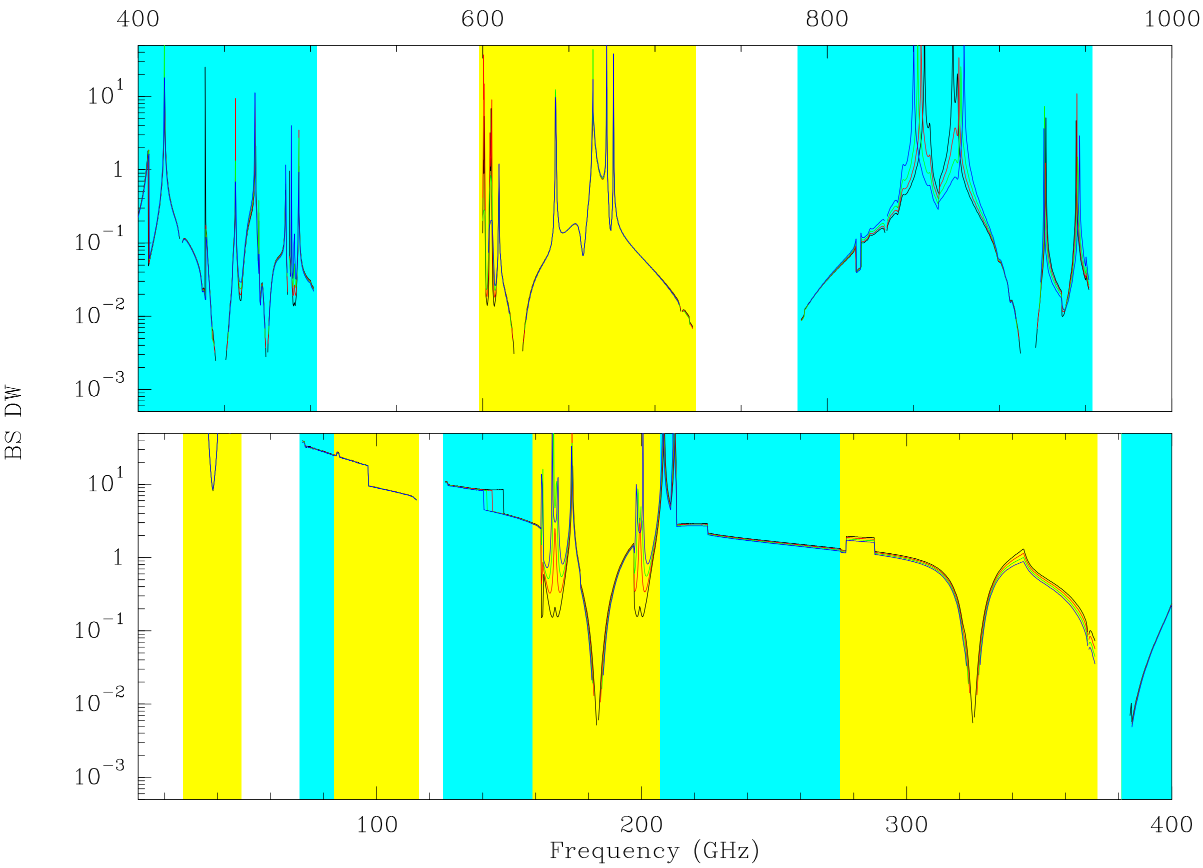


Figure 5: Maximum frequency offset to preserve a bandpass error of 0.1 % despite errors on the water vapor content in a Single Load calibration. The assumed error on water content is 0.1 mm.

### 2.4.4 Bandpass error in Single Load calibration

Figures 4, 5 and 6 give the maximum frequency offset which can be tolerated before the bandpass error exceeds 0.1% for the Single Load calibration. Figure 4 is for the airmass difference of 0.5. Figure 5 is for a water vapor error of 0.1 mm. Figure 6 is for an atmospheric temperature error of 1 K.

### 2.4.5 Bandpass error in Dual Load calibration

The same parameters can be computed for the Dual Load calibration. However, the $T_{\rm cal}$ factor has no dependence in temperature for the dual-load calibration (see Eq.28), so there are no

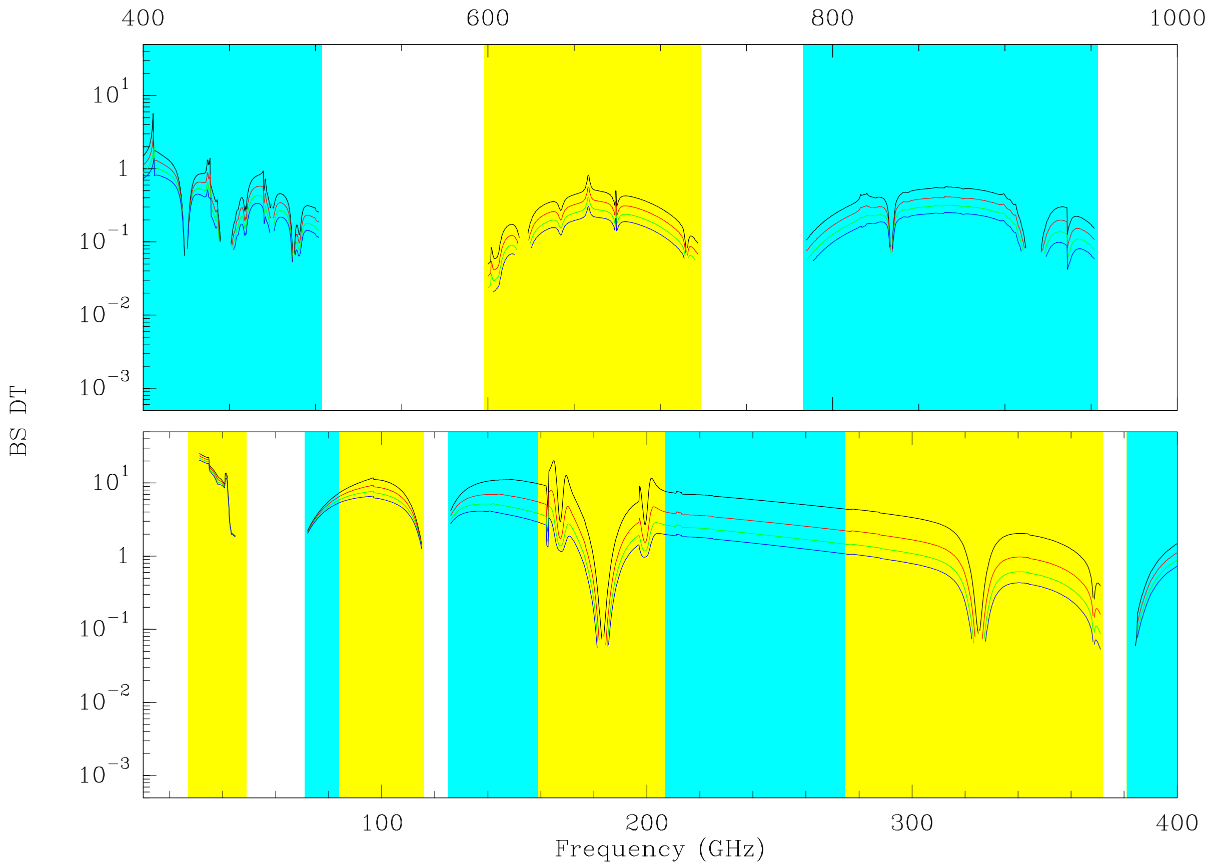


Figure 6: Maximum frequency offset to preserve a bandpass error of 0.1 % despite errors on the atmospheric temperature $J_{\rm m}$ in a Single Load calibration. The assumed error on temperature is 1 K.

errors associated with the temperature. Figure 7 is for the airmass difference of 0.5. Figure 8 is for a water vapor error of 0.1 mm.

### 2.4.6 Comparison

To figure out which method is advantageous, it is practical to display the ratio of permissible frequency offsets for Single Load over that for Dual Load. Ratios larger than 1 indicate that the Single Load method is more appropriate. This ratio is presented for the two common errors in Fig. 9-10.

It can be seen from the Fig.9-10 that the Single Load calibration provides significantly better accuracy than the Dual Load calibration method over most of the frequency coverage. This remains true unless the error on the atmospheric temperature $J_{\rm m}$ significantly exceeds a few K (see Fig.6).

## 2.5 Integration Times and Source Strength

From Eqs.29 and 22, it can be seen that the error on $T_A(\nu)$ depends not only on $T_{\rm cal}$ but also on the noise on $P_{\rm load}$ and $P_{\rm sky}$ (or $P_{\rm hot}$ and $P_{\rm cold}$ for the dual load case). These errors must be kept small compared to the noise on $C_{\rm source}$. The time which must be spent calibrating the amplitude (i.e. measuring $P_{\rm load}$ and $P_{\rm sky}$) will thus depend on the (correlated) source strength.

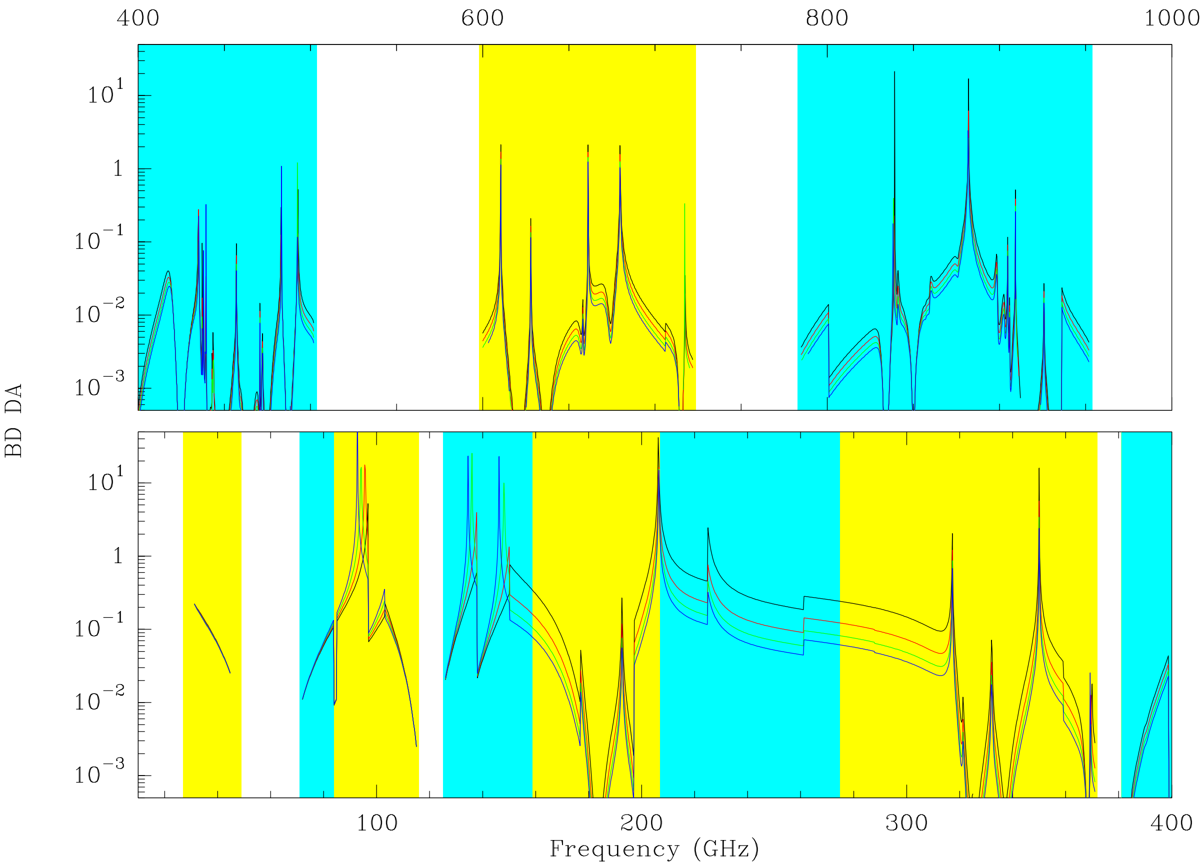


Figure 7: Maximum frequency offset to preserve a bandpass error of 0.1 % despite the elevation change between the source and the bandpass calibration for the Dual Load calibration The assumed elevation change is 0.5 airmass.

In most cases, the source strength is a small fraction of the noise power. Since we must calibrate the amplitude frequently to correct for the atmospheric opacity fluctuations, the restriction on the integration time for the amplitude calibration are small. For example, a 30 Jy source is only 1 or 2 % of the system temperature, so calibrating for 1 second every 2 to 5 minutes would be more than sufficient.

The worst case would be observations of strong sources, for example maser lines or planets. Moreover, in this calibration scheme, it is assumed that $P_{\mathrm{sky}}$ is the power on the empty sky, without any source contribution. This can be obtained by dedicated observations of an empty region of the sky near the source (for example when observing planets) or, in the case of spectral lines, by interpolation of the power from empty regions of the spectrum.

Finally, the integration time on the bandpass calibrator is directly dependent on the ratio of calibrator strength over source strength, and should be adjusted accordingly for each project.

## 2.6 Discussion

Fig.4-6 demonstrate that bandpass accuracies of 0.1 % can be reached over bandwidth ranging from 100 MHz (near atmospheric absorption lines) to 10 GHz and even beyond. Since the bandpass error is strictly proportional to the frequency difference, proportionally higher accuracy can be reached over narrower bandwidths.

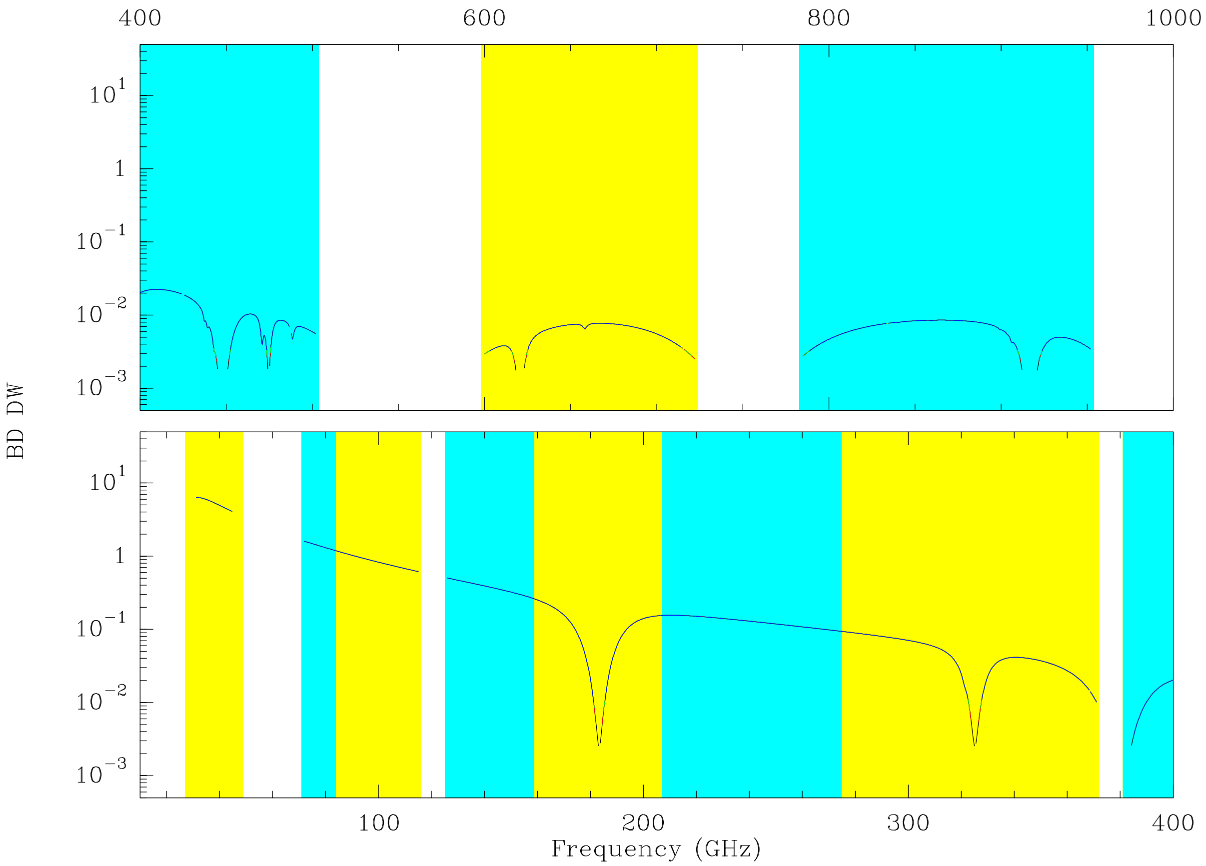


Figure 8: Maximum frequency offset to preserve a bandpass error of 0.1 % despite errors on the water vapor content in Dual Load calibration. The assumed error on water content is 0.1 mm.

Interpreting Fig.4-6 requires some care. For example, the accuracy seems limited at submm wavelengths. However, the assumption of 0.1 mm of error on the water vapor is certainly significantly larger than what can be done when the water vapor content is in the range 0.35 – 0.65 mm, and the bandpass error displayed in Fig.5 scales linearly with this assumed error. Also, the interpretation of the frequency difference is difficult. In the figures, we assumed the calibration was made at one (sampled) frequency, while the observation is done at a slightly different frequency. In practice, because of the requirement of sufficient signal to noise in the measurement of $X_{\rm source}(\nu)$, the bandpass will be determined by using an average over a finite bandwidth. Because of this averaging effect, a first order estimate is that the effective bandwidth over which the precision is obtained is 4 times larger than the frequency quoted in the Figures (or equivalently that the bandpass accuracy is actually 4 times better for this bandwidth).

Finally, the ATM model used here does not contain a number of minor constituents like Ozone, so that a significant number of narrow lines will need to be added and will modify the details of the bandpass accuracy. This is expected to be insignificant below 220 GHz, but will limit the accuracy (near these lines) at sub-mm wavelengths.

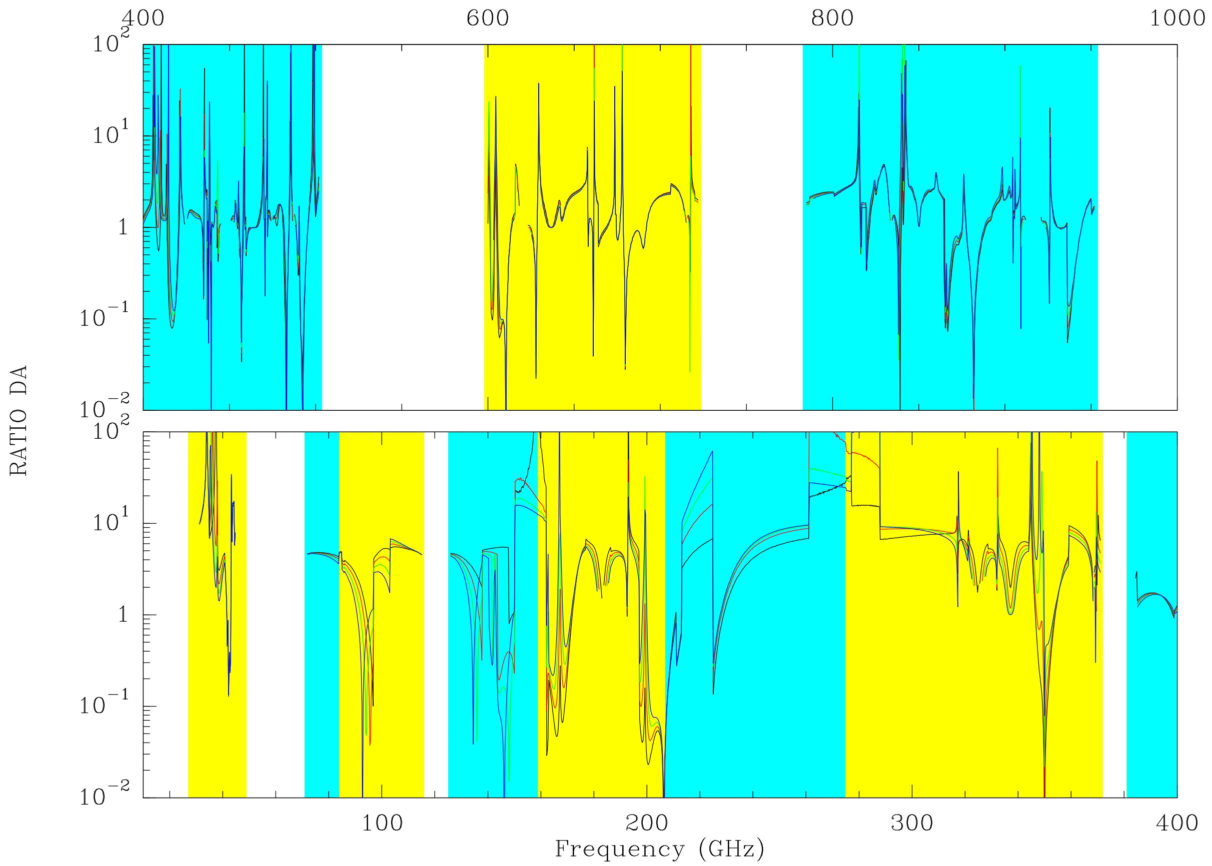


Figure 9: Ratio of allowable bandwidth for the same bandpass error in Single Load and Dual Load calibration schemes, for the elevation difference between the source and the calibrator.

# 3 Gain ratio measurement

A special case of the bandpass calibration is the sideband gain ratio $g$, that is $g(\nu_{\rm Signal})/g(\nu_{\rm Image})$ for $\nu_{\rm Signal}$ and $\nu_{\rm Image}$ corresponding to the same $\nu_{\rm RF}$. $g$ is required to compute the calibration temperatures $T_{\rm cal}$ (see Eq.21 and 29).

## 3.1 Equations

The cross correlation gives the source temperature in both sidebands, $T_A^s$ for the signal sideband and $T_A^i$ for the image sideband.

$$T_A^s = T^s_{cal1} \times \frac{C^s_{\rm source}}{P_{\rm load} - P_{\rm sky}} = T^s_{cal2} \times \frac{C^s_{\rm source}}{P_{\rm hot} - P_{\rm cold}} \tag{54}$$

$$T_A^i = \frac{T^s_{cal1}}{g} \times \frac{C^i_{\rm source}}{P_{\rm load} - P_{\rm sky}} \times e^{-(\tau_s - \tau_i)} = \frac{T^s_{cal2}}{g} \times \frac{C^i_{\rm source}}{P_{\rm hot} - P_{\rm cold}} \times e^{-(\tau_s - \tau_i)} \tag{55}$$

where $g$ is the gain ratio (ratio of the gains $g^i$ in the image sideband and $g^s$ in the signal sideband, normalized so that $g^i + g^s = 1$), $C_{\rm source}$ is the correlated signal from the source, $P_{\rm load}$ and $P_{\rm sky}$ the output power measured on the load and on the sky, respectively, and $T_{\rm cal1}$ the calibration temperature for Single Load, and $T_{\rm cal2}$ for Dual Load. The superscripts $i$ and $s$ stand for the image sideband and signal sideband, respectively.

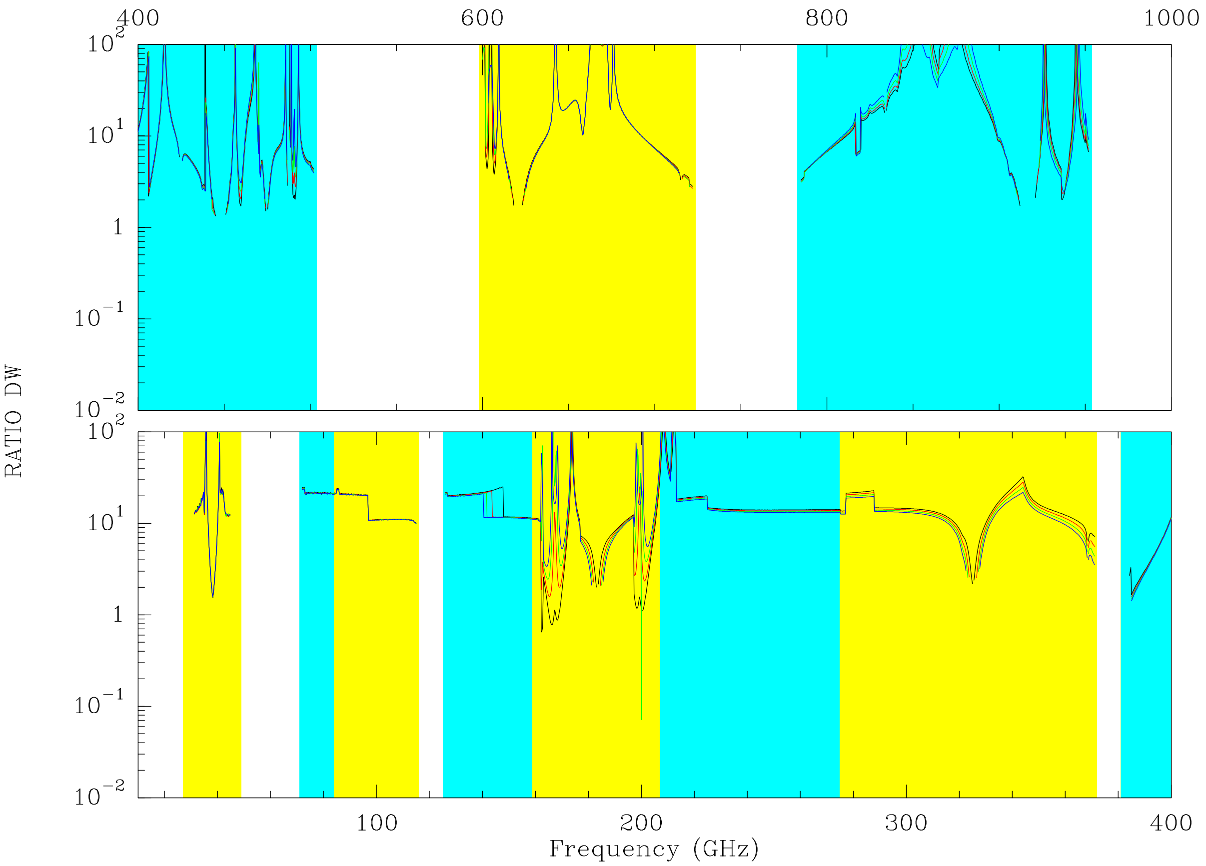


Figure 10: Ratio of allowable bandwidth for the same bandpass error in Single Load and Dual Load calibration schemes, for the errors on the water vapor content.

By taking the ratio of the temperatures in the signal and in the image sideband:

$$\frac{T_A^s}{T_A^i} = g\,\frac{C^s_{\text{source}}}{C^i_{\text{source}}} \times e^{(\tau_i - \tau_s)} \tag{56}$$

$$g = \left(\frac{T_A^s}{T_A^i}\right)\frac{C^i_{\text{source}}}{C^s_{\text{source}}} e^{(\tau_s - \tau_i)} \tag{57}$$

we can derive $g$. In the case of a continuum source, the ratio of the temperatures only depends on the spectral index of the source, and is close to 1 since the difference in frequency between the signal and image bands is small compared to either frequency. The precision on $g$ will thus depend on the precision on $\tau_s - \tau_i$ and on the knowledge of the bandpass calibrator spectral index. Note that the above expression is independent of the calibration scheme.

### 3.2 Opacity Prediction

The opacity difference, $\tau_s - \tau_i$, can be obtained from the predictive atmospheric model like ATM. Another solution however is when 2 calibration sources at 2 different elevations can be observed. In this case, $\tau_s - \tau_i$ can be *measured.*

### 3.2.1 Opacity Difference Measurement

If $a$ is the airmass through which the first source $A$ is observed and $b$ the airmass through which the other source $B$ is observed, we can write

$$g = \frac{T_A^s(A)}{T_A^i(A)} \frac{C_{source}^i(A)}{C_{source}^s(A)} \times e^{(\tau_s^0-\tau_i^0)a} \tag{58}$$

$$g = \frac{T_A^s(B)}{T_A^i(B)} \frac{C_{source}^i(B)}{C_{source}^s(B)} \times e^{(\tau_s^0-\tau_i^0)b} \tag{59}$$

where $\tau_s^0$ and $\tau_i^0$ are the signal and image zenith opacities. With this system of 2 equations and 2 unknowns $(\tau_s^0 - \tau_i^0)$ and $g$, $g$ can be determined without assumptions on the opacity:

$$g = \frac{T_A^s(A)}{T_A^i(A)} \frac{C_{source}^i(A)}{C_{source}^s(A)} \left[\frac{T_A^s(B)}{T_A^i(B)} \frac{T_A^i(A)}{T_A^s(A)} \frac{C_{source}^i(B)}{C_{source}^s(B)} \frac{C_{source}^s(A)}{C_{source}^i(A)}\right]^{\frac{a}{a-b}} \tag{60}$$

The calibration sources have to be sources of flat spectrum or of known spectral index. If we call $\alpha$ the spectral index of source $A$ and $\beta$ the spectral index of source $B$, then:

$$\frac{T_A^s(A)}{T_A^i(A)} = \left(\frac{\nu_s}{\nu_i}\right)^\alpha$$

$$\frac{T_A^s(B)}{T_A^i(B)} = \left(\frac{\nu_s}{\nu_i}\right)^\beta$$

where $\nu_s$ and $\nu_i$ are the signal and image frequencies. Since we consider only the ratio of the source temperatures in the signal and in the image band, it is not necessary to know the flux of the calibrator.

### 3.2.2 Measurement precision

Eq. (60) can be rewritten as the product of two terms, $g_T$ and $g_c$, one coming from the knowledge of the temperature ratios ($g_T$), the other from the measurements of the correlated intensities ($g_c$):

$$g = \underbrace{\frac{T^s(A)}{T^i(A)} \left[\frac{T^s(B)}{T^i(B)} \frac{T^i(A)}{T^s(A)}\right]^{\frac{a}{a-b}}}_{g_T} \underbrace{\frac{C^i(A)}{C^s(A)} \left[\frac{C^i(B)}{C^s(B)} \frac{C^s(A)}{C^i(A)}\right]^{\frac{a}{a-b}}}_{g_c}$$

and the error on $g$ derived:

$$\frac{\delta g}{g} = \frac{\delta g_T}{g_T} + \frac{\delta g_c}{g_c} \tag{61}$$

- For $g_T$ we have:

$$\frac{\delta g_T}{g_T} = \left|\ln\left(\frac{\nu_s}{\nu_i}\right)\right| \delta\alpha + \frac{a}{|a-b|} \left(\left|\ln\left(\frac{\nu_s}{\nu_i}\right)\right| \delta\beta + \left|\ln\left(\frac{\nu_s}{\nu_i}\right)\right| \delta\alpha\right) \tag{62}$$

Assuming equal uncertainties on the spectral index of both calibration sources ($\delta\alpha = \delta\beta$), and neglecting the fact that these uncertainties may be uncorrelated:

$$\frac{\delta g_T}{g_T} = \left(1 + \frac{2a}{|a-b|}\right) \left|\ln\left(\frac{\nu_s}{\nu_i}\right)\right| \delta\alpha \tag{63}$$

- For $g_c$:

$$\left(\frac{\delta g_c}{g_c}\right)^2 = \left(\frac{\delta C^i(A)}{C^i(A)}\right)^2 + \left(\frac{\delta C^s(A)}{C^s(A)}\right)^2 + \left(\frac{a}{a-b}\right)^2 \left[\left(\frac{\delta C^s(A)}{C^s(A)}\right)^2 + \left(\frac{\delta C^i(A)}{C^i(A)}\right)^2 + \left(\frac{\delta C^s(B)}{C^s(B)}\right)^2 + \left(\frac{\delta C^i(B)}{C^i(B)}\right)^2\right] \tag{64}$$

To first order, the correlator signal in the image band is linked to that in the signal band by: $C^i \simeq g\ C^s$ (since $T^i/T^s \sim 1$ and $\tau_i \sim \tau_s$). The noise on this signal is the same in both bands: $\delta C^i = \delta C^s$. Therefore:

$$\frac{\delta C^i}{C^i} = \frac{1}{g}\frac{\delta C^s}{C^s}$$

If in addition we suppose similar measurement errors for both calibration sources, ie.

$$\frac{\delta C^s(A)}{C^s(A)} = \frac{\delta C^s(B)}{C^s(B)} = \frac{\delta C^s}{C^s}$$

Eq. 64 becomes:

$$\left(\frac{\delta g_c}{g_c}\right)^2 = \left(\frac{1+g^2}{g^2}\right)\left(1+2\left(\frac{a}{a-b}\right)^2\right)\left(\frac{\delta C^s}{C^s}\right)^2 \tag{65}$$

### 3.2.3 Error on $g$

Since we have $g_T \approx 1$ and $g_c \approx g$, we can write:

$$\frac{\delta g}{g} \simeq \delta g_T + \frac{\delta g_c}{g}$$

The expression of $\delta g$ depends upon whether the receivers are SSB or DSB.

- and in SSB, $g \ll 1$, ie

$$\delta g \approx g\,\delta g_T + \delta g_c \approx \delta g_c$$

- In DSB mode, $g \simeq 1$, so that

$$\delta g \approx \delta g_T + \delta g_c$$

To evaluate $\delta g_T/g_T$, we can use the approximate relation:

$$\ln\left(\frac{\nu_i}{\nu_s}\right) \sim \frac{2\,\nu_{IF}}{\nu_i}$$

with $\nu_{IF}$ ranging from 4 to 12 GHz, depending on the receiver band and where in the IF band we are looking at.

Using $\nu_{IF} = 8$ as an average, and taking typical values for the airmasses, e.g. $a = 1.7$ and $|a-b| = 0.5$ (i.e. $b = 1.2$ or $b = 2.2$), and assuming an uncertainty on the spectral index of $4\,10^{-2}$, we find:

$$\frac{\delta g_T}{g_T} \sim \delta g_T \sim 1.25/\nu\ [\mathrm{GHz}]$$

and for $g_c$:

$$\delta g_c = \sqrt{(1+g^2)\left(1+2\left(\frac{a}{a-b}\right)^2\right)}\,\frac{\delta C^s}{C^s}$$

### 3.2.4 Improvement of precision

The precision on $g$ can be better than given by the equations above, since the zenith opacity difference between the signal sideband and image sideband $\tau_s^0 - \tau_i^0$ can be considered to be the same for each antenna of the array [1]. This means that the $N$ systems of Eq. 58 and 59 yielding the antenna gain ratio $g$ for an antenna have a common unknown $\tau_s^0 - \tau_i^0$. Therefore, the random part of the error on $\tau_s^0 - \tau_i^0$ can be reduced by a factor $\sqrt{N}$, and the precision on $g$ can be improved as well (Eq. 58).

From Eq. 58 and 59, the opacity difference in the signal and in the image sideband can be written as:

$$\tau_s^0 - \tau_i^0 = \frac{1}{a-b}\left[\ln\left(\frac{T_A^s(B)}{T_A^i(B)}\frac{T_A^i(A)}{T_A^s(A)}\right) + \ln\left(\frac{C^i(B)}{C^s(B)}\frac{C^s(A)}{C^i(A)}\right)\right] \tag{66}$$

Using the for the opacities the same decomposition as for $g$, i.e.: $\tau_s^0 - \tau_i^0 = \tau = \tau_T + \tau_c$ with

$$\tau_T = \frac{1}{a-b}\ln\left[\frac{T_A^s(B)}{T_A^i(B)}\frac{T_A^i(A)}{T_A^s(A)}\right] \tag{67}$$

$$\tau_c = \frac{1}{a-b}\ln\left[\frac{C^s(A)}{C^i(A)}\frac{C^i(B)}{C^s(B)}\right] \tag{68}$$

the errors on $\tau_c$ and $\tau_T$ can be written as:

$$\delta\tau_T = \left|\ln\left(\frac{\nu^s}{\nu^i}\right)\right| \times \frac{\delta\alpha + \delta\beta}{|a-b|} \tag{69}$$

$$(\delta\tau_c)^2 = \left(\frac{1}{a-b}\right)^2\left[\left(\frac{\delta C^s(B)}{C^s(B)}\right)^2 + \left(\frac{\delta C^i(B)}{C^i(B)}\right)^2 + \left(\frac{\delta C^s(A)}{C^s(A)}\right)^2 + \left(\frac{\delta C^i(A)}{C^i(A)}\right)^2\right] \tag{70}$$

Making the same assumptions on $\delta\alpha$, $\delta\beta$ and $\delta C/C$ yields:

$$\delta\tau_T \simeq 2\left|\ln\left(\frac{\nu^s}{\nu^i}\right)\right| \frac{\delta\alpha}{|a-b|} \tag{71}$$

$$\delta\tau_c \simeq \frac{\sqrt{2}}{a-b}\,\frac{\sqrt{1+g^2}}{g}\,\frac{\delta C^s}{C^s} \tag{72}$$

While the precision on $\tau_T$ is limited by the knowledge of the source spectral index, with $N$ antennas, we have $N$ independent measurements of $\tau_c$. Assuming all antennas have receivers with similar values for $g$ and similar system temperatures yielding similar $\delta C/C$, Eq.72 becomes:

$$\delta\tau_c \simeq \frac{\sqrt{2}}{a-b}\,\frac{\sqrt{1+g^2}}{g}\,\frac{1}{\sqrt{N}}\,\frac{\delta C^s}{C^s} \tag{73}$$

The errors for $\tau_T$, and $\tau_c$ after the precision improvement obtained with $N = 64$ are given in Table 1. These errors were obtained supposing the SSB gain is 15 dB. At mm wavelengths, the impact of the uncertainty in the spectral index is limited by the sideband rejection. At submm wavelengths, where receivers are DSB, it is limited by the small relative difference in frequency between both sidebands.

[1] In the largest configurations, the **opacities** may vary significantly from one antenna to the other. However, the **opacity differences** between the two sidebands are often due to relatively stable components of the atmosphere ($O_2$, ozone), and are likely to be much less variable with antennas.

| $\nu$ [GHz] | 90 | 230 | 350 | 410 | 690 | 850 |
|---|---|---|---|---|---|---|
| $g\,\delta\tau_T$ | $9.0\,10^{-4}$ | $3.5\,10^{-4}$ | $2.3\,10^{-4}$ | $6.2\,10^{-3}$ | $3.7\,10^{-3}$ | $3.0\,10^{-3}$ |
| $g\,\delta\tau_c/(\delta C^s/C^s)$ | 0.35 | 0.35 | 0.35 | 0.5 | 0.5 | 0.5 |

Table 1: Error on $\tau_T$ and $\tau_c$ defined in Eq. 67 and 68, such as the zenith opacity difference $\tau = \tau_s^0 - \tau_i^0 = \tau_T + \tau_c$. The error on $\tau_c$ takes into account the improvement due to the $N$ antennas. The receivers are supposed SSB up to 350 GHz. In SSB, the gain $g$ was taken as 0.03 (15 dB).

Now that we have derived the error on $\tau_s - \tau_i$, we can estimate the error on the gain $g$. We introduce $\gamma_T$ and $\gamma_c$ in Eq. 58:

$$\gamma_T = \frac{T^s(A)}{T^i(A)} \text{ and } \gamma_c = \frac{C^i(A)}{C^s(A)} \tag{74}$$

so that: $g = \gamma_T\,\gamma_c\,e^{a\,\tau}$, and

$$\begin{aligned}
g &= (\gamma_T\,e^{a\tau_T})\,(\gamma_c\,e^{a\tau_c}) \\
\frac{\delta g}{g} &= \frac{\delta\gamma_T}{\gamma_T} + a\,\delta\tau_T + \sqrt{\left(\frac{\delta\gamma_c}{\gamma_c}\right)^2 + (a\,\delta\tau_c)^2} \\
\frac{\delta\gamma_T}{\gamma_T} &= \left|\ln\left(\frac{\nu^s}{\nu^i}\right)\right| \times \delta\alpha \\
\left(\frac{\delta\gamma_c}{\gamma_c}\right)^2 &= \left(\frac{\delta C^s(A)}{C^s(A)}\right)^2 + \left(\frac{\delta C^i(A)}{C^i(A)}\right)^2 = \frac{1+g^2}{g^2}\left(\frac{\delta C^s}{C^s}\right)^2
\end{aligned}$$

which yields:

$$\begin{aligned}
\frac{\delta g}{g} &= \left|\ln\left(\frac{\nu^s}{\nu^i}\right)\right| \delta\alpha + a\,\delta\tau_T + \sqrt{\frac{1+g^2}{g^2}\left(\frac{\delta C^s}{C^s}\right)^2 + a^2\,(\delta\tau_c)^2} \\
&= \left|\ln\left(\frac{\nu^s}{\nu^i}\right)\right| \delta\alpha + a\,\delta\tau_T + \frac{\sqrt{1+g^2}}{g}\sqrt{1+\frac{2\,a^2}{N(a-b)^2}}\,\frac{\delta C^s}{C^s}
\end{aligned} \tag{75}$$

so that :

$$g\,\delta g_T = g\left|\ln\left(\frac{\nu^s}{\nu^i}\right)\right| \delta\alpha + a\,g\delta\tau_T \tag{76}$$

$$\delta g_c = \sqrt{1+g^2}\sqrt{1+\frac{2\,a^2}{N(a-b)^2}}\,\frac{\delta C^s(A)}{C^s(A)} \tag{77}$$

Expanding the error on $\tau_T$ from Eq.71, we obtain

$$g\,\delta g_T = g\left|\ln\left(\frac{\nu^s}{\nu^i}\right)\right|\left(1+\frac{2a}{|a-b|}\right)\delta\alpha \tag{78}$$

$$\delta g_c = \sqrt{1+g^2}\sqrt{1+\frac{2}{N}\left(\frac{a}{a-b}\right)^2}\,\frac{\delta C^s}{C^s} \tag{79}$$

The original case with $N = 1$ (which was unphysical, since at least 3 antennas are required to determine an antenna-based gain) is included in this more general expression.

The final outcome depends on the value of $g$:

- for SSB receivers, $g \ll 1$

$$\delta g = g \left| \ln\left(\frac{\nu^s}{\nu^i}\right) \right| \left(1 + \frac{2a}{|a-b|}\right) \delta\alpha + \sqrt{1 + \frac{2}{N}\left(\frac{a}{a-b}\right)^2} \frac{\delta C^s}{C^s} \tag{80}$$

- in DSB, $g \sim 1$

$$\delta g = \left| \ln\left(\frac{\nu^s}{\nu^i}\right) \right| \left(1 + \frac{2a}{|a-b|}\right) \delta\alpha + \sqrt{2}\sqrt{1 + \frac{2}{N}\left(\frac{a}{a-b}\right)^2} \frac{\delta C^s}{C^s} \tag{81}$$

Table 2 gives the final error on $g$, assuming $g = 0.03$ for mm bands, and $g = 1$ for the sub-mm receivers, and $N = 64$.

| $\nu$ [GHz] | 90 | 230 | 350 | 410 | 690 | 850 |
|---|---|---|---|---|---|---|
| $g\,\delta g_T$ | $1.8\,10^{-3}$ | $6.8\,10^{-4}$ | $4.5\,10^{-4}$ | $1.2\,10^{-2}$ | $7.2\,10^{-3}$ | $5.9\,10^{-3}$ |
| $\delta g_c/(\delta C^s(A)/C^s(A))$ | 1.17 | 1.17 | 1.17 | 1.65 | 1.65 | 1.65 |

Table 2: Errors $g\,\delta g_T$ and $\delta g_c$ ($\delta g = g\,\delta g_T + \delta g_c$), taking into account the fact that the precision on $\tau_c$ can be improved by a factor $\sqrt{N} = 8$. In SSB, the gain $g$ was taken to be 15 dB.

Since $\delta g = g\,\delta g_T + \delta g_c$, a precision on $g$ of 1% at millimeter wavelengths and of 3% at submillimeter wavelengths is obtained for the precision on $\delta C^s/C^s$ given in Table 3.

Table 3: Signal to noise (at the signal frequency, $SNR = C^s/\delta C^s$) needed to obtain a precision on $g$ of 1 % at millimeter wavelengths and 3 % at submillimeter wavelengths.

| $\nu$ [GHz] | 90 | 230 | 350 | 410 | 690 | 850 |
|---|---|---|---|---|---|---|
| $\delta g$ | 1 % | 1 % | 1 % | 3 % | 3 % | 3 % |
| $\frac{\delta C^s}{C^s}$ | 0.70 % | 0.80 % | 0.82 % | 1.09 % | 1.38 % | 1.46 % |
| $SNR$ | 143 | 126 | 123 | 92 | 72 | 68 |

### 3.2.5 Integration time

The sensitivity which can be obtained on the correlation coefficient is given by

$$\frac{\delta C^s}{C^s} = \frac{\sigma_0}{\sqrt{\Delta\nu\, t}\; S_\nu} \tag{82}$$

(cf. ALMA Memo 372, Eq. 8). $\sigma_0$ is the antenna based sensitivity given in Table 6 of Memo 372. The integration times to reach the precision given in Table 3 for $\delta C^s/C^s$ in the different frequency bands are presented in Table 4, for source intensities of 1.5 Jy and 1 Jy, and a frequency resolution of 250 MHz. The actual calibration time is twice the values given in Table 4 since two calibrators must be observed.

| $\nu$ [GHz] | 90 | 230 | 350 | 410 | 690 | 850 |
|---|---|---|---|---|---|---|
| $\sigma_0$ (mJy) | 14.2 | 30.9 | 75.9 | 93.2 | 319.5 | 399.3 |
| $t_{int}$(1 Jy) | 16 s | 1 min | 6 min | 4 min 45 s | 35 min | 47 min |
| $t_{int}$(1.5 Jy) | 7 s | 27 s | 2 min 40 s | 2 min 10 s | 15 min 25 s | 21 min |

Table 4: Needed integration times to reach the value given in Table 3 on the precision of $g$ over a 250 MHz bandpass for a calibration source of 1 Jy and a calibration source of 1.5 Jy. Values for $\sigma_0$ are taken from Table 6 of Memo 372.

### 3.3 Discussion

The error on $g$ mentioned in Table 2 is an **absolute** error, and should **not** be interpreted as a bandpass error. Indeed, it is expected that $g$ is only slowly dependent on the (IF) frequency, since the intrinsic bandwidth of the receiver is large[2]. However, apparent variations of $g$ on smaller scales can be obtained since the measurement process directly links $g$ to $\tau_s - \tau_i$, which can have narrow features due for example to the Ozone lines. It is thus important in the determination of $g$

- to use the best possible prediction of $\tau_s - \tau_i$ at the adequate spectral resolution.
- to solve for $g$ at a coarser frequency resolution only once this opacity correction has been properly applied.

If needed, an iterative process can be implemented (progressively increasing the resolution for $\tau_s - \tau_i$, but decreasing it for $g$). Remaining small errors on $g$ as a function of frequency will be corrected by the bandpass calibration. This is valid in an *a posteriori* calibration process, where it is indeed possible to obtain a suitable bandpass calibration source. In case no strong enough source can be found to measure the bandpass, i.e. in an *a priori* calibration scheme, the distinction between the bandpass error and the error on $g$ becomes less significant (the bandpass is then $g(\nu)/ < g(\nu) >$).

## 4 Phase Bandpass Calibration

The previous section only dealt with amplitude. Phase bandpass can only be measured using a common signal injected into all antennas. In some arrays, such a common signal can be injected fairly high in the signal path: for example, a common noise source can be switched into all antenna ports of the correlator in the IRAM array. This gives 100 % correlation, and allows to calibrate with high spectral resolution the details of the frequency response in phase of the correlator. One is then left with the phase response coming from the other parts of the instrument, i.e. cables, receivers and antennas, but which have a much shallower frequency dependence.

Because the signal is digitized at the antenna in ALMA, this is unfortunately not possible. The only "common signal" is a reference astronomical source. Then, the measurement will be signal to noise limited. However, the situation is not as bad as it looks. The reason is that all processing after digitization is pure numeric (by definition), so that its effect on the bandpass can be predicted. Hence, we are left with calibrating signals over bandwidths of order 1 GHz, since the sampling is done in the 2-4 GHz band.

[2]This can be assessed by looking at the predicted response of each receiver cartridge

Simulations of the anti-aliasing filter response have been performed by [d'Addario, memo 452]. From the Figure 6 of this memo, we can derive a maximum phase change going as $\sim 180^\circ(\delta\nu/0.5\text{ GHz})^2$ near the filter edges.

$$\delta\phi \leq 180^\circ \left(\frac{\delta\nu}{\Delta\nu_T}\right)^2 \tag{83}$$

with $\Delta\nu_T = 0.5$ GHz. Thus if we want to limit the phase error to say $\phi_e = 1^\circ$, we have to calibrate the phase at a resolution $\Delta\nu$ such that

$$\left(\frac{\Delta\nu}{\Delta\nu_T}\right)^2 \leq \frac{\phi_e}{180^\circ} \tag{84}$$

$$\Delta\nu \leq \Delta\nu_T\sqrt{\frac{\phi_e}{180^\circ}} \tag{85}$$

which gives 40 MHz for $\phi_e = 1^\circ$. Now, we also want the random error on the phase during the calibration to be less than the same value. Since the phase error $\sigma_\phi$ is related to the antenna sensitivity by

$$\sigma_\phi \text{ (deg)} = \frac{180^\circ}{\pi}\frac{\sigma_0}{S_\nu\sqrt{t\Delta\nu}} \tag{86}$$

(see ALMA Memo 372, Eq.6), we thus need

$$t = \left(\frac{180^\circ}{\pi\phi_e}\right)^2 \frac{1}{\Delta\nu}\left(\frac{\sigma_0}{S_\nu}\right)^2 \tag{87}$$

$$t = \left(\frac{180^\circ}{\phi_e}\right)^{5/2} \frac{1}{\pi^2\Delta\nu_T}\left(\frac{\sigma_0}{S_\nu}\right)^2 \tag{88}$$

If we want to equally balance the random and systematic error in the budget, the value of $\phi_e$ in these formulas should be $\sqrt{2}$ lower than the desired goal. Table 5 gives the expected integration time as function of frequency for a 1° final error and 3° also. Note that the integration time goes as the 5/2 power of the required precision.

| $\nu$ [GHz] | 90 | 230 | 350 | 410 | 690 | 850 |
|---|---|---|---|---|---|---|
| $\sigma_0$ (mJy) | 14.2 | 30.9 | 75.9 | 93.2 | 319.5 | 399.3 |
| $t_{int}$(1 Jy) | 17 s | 1 min 24 s | 8 min 30 s | 13 min | 2 h 30 min | 4 h |
| $t_{int}$(1 Jy) | 1.1 s | 5.4 s | 33 s | 49 s | 9 m 40 s | 15 min |

Table 5: Needed integration times to reach 1° overall bandpass error when observing a 1 Jy source as a calibrator (line 2). Line 3 gives the time required to obtain 3° bandpass error only. Values for $\sigma_0$ are taken from Table 6 of Memo 372.

# 5 Conclusion

We have shown that bandpass calibration with an accuracy of 0.1 % is possible on astronomical sources provided the electronic is made sufficiently stable and standing waves are minimized, making the atmosphere the ultimate limiting factor. Since astronomical sources have to be used, the required integration time varies substantially as a function of frequency. High accuracies can be reached in a minute of time at mm wavelengths, but integration time as large as an hour can be needed at sub-mm wavelengths.

We can minimize the bandpass errors due to the atmosphere by using a scheme based on the single-load amplitude calibration. The proposed scheme is a variant of the so-called bandpass normalization technique. It uses normalization by the difference between the sky emission and the load emission, rather than normalization by the auto-correlation spectrum in the usual case.

In this scheme, the calibration factor $T_{\mathrm{cal}}$ should be computed with sufficient spectral resolution to represent the variations of the atmospheric opacity with frequency. Using the single-load expression for $T_{\mathrm{cal}}$ result in a smoother dependence with frequency, which is more amenable to interpolation than the dual-load expression. Whenever the correlator is configured into narrow bands, it can be advantageous to perform the bandpass calibration in broad band mode only to improve the accuracy of the atmospheric modelling, since the $T_{\mathrm{cal}}$ and hence $B(\nu)$ factors are solely functions of frequency (see Eq.53).

To calibrate out the fine structure of the bandpass, which is due to the electronics, we propose to make direct use of the known properties of the digital filters. The response (in amplitude and phase) of these filters will have to be calculated (and if possible measured once in the laboratory) and to be inserted in the calibration software.

Bandpass calibration must be performed at the observing frequency. It will be limited by the knowledge of the sideband opacity difference. This could be significant near the edges of atmospheric lines. This situation is more frequent in the sub-mm domain, where the number of lines from minor constituents like Ozone is larger. The sideband opacity difference can be predicted from the atmospheric model. However, a direct measurement is also possible, by using two bandpass calibrators at different elevations. Such measurements can be time consuming (specially at sub-mm frequencies), but could be used occasionally to improve the accuracy of the atmospheric model.

The bandpass calibration must be performed on strong point-like sources, of known spectral index. The knowledge of the spectral indexes will be a limiting factor in the wide band modes. Building up a database of suitable sources will be necessary, since the knowledge of these spectral indexes could be improved by bootstrapping techniques among several sources. The list of calibrators should be large enough, because even the spectral index is likely to vary as a function of time for quasars.

# References

[Mangum memo 318]
Mangum, J. 2000
Amplitude Calibration at Millimeter and Sub-millimeter Wavelengths *ALMA memo 318*

[Plambeck memo 321]
Plambeck, R., 2000
Receiver Amplitude Calibration for ALMA *ALMA memo 321*

[Bock et al. memo 225]
Bock, D., Welch, W.J., Fleming, M. & Thornton D., 1998
Radiometric Calibration at the Cassegrain Secondary Mirror *ALMA memo 225*

[Tucker & Feldman 1985]
Tucker, J.R, Feldman, M.J. 1985
Quantum Detection at Millimeter Wavelengths
Review of Modern Physics, 57, 1055-1113

[Ulich & Haas, 1976]
Ulich, R. & Haas, R.W., 1976
Amplitude Calibration of Millimeter Wavelengths Spectral Lines
ApJ Supp. 30, 247

[Guilloteau & Moreno, memo 371]
Moreno, R., & Guilloteau, S. 2001,
Receiver Calibration Schemes for ALMA *ALMA memo 371*

[Moreno & Guilloteau, memo 372]
Moreno, R., & Guilloteau, S. 2002,
ALMA Calibration: Requirements on the integration times, and suggested observing strategies. *ALMA memo 372*

[Kerr memo 401]
Kerr, A.R., 2002
Saturation by Noise and CW Signals in SIS Mixers. *ALMA memo 401*

[Guilloteau, memo 423]
Guilloteau, S.,
The vane calibration system revisited. *ALMA memo 423*

[d'Addario, memo 452]
d'Addario, L.,
Passband Shape Deviation Limits. *ALMA memo 452*